PHOTONICS Research

Regenerated polymer optical fiber Bragg gratings with thermal treatment for high temperature measurements

Dinusha Serandi Gunawardena,[1,2,3] Xin Cheng,[1,2,4] Jingxian Cui,[1,2] Geraldi Edbert,[1] Linyue Lu,[1,2] Yuk Ting Ho,[1] and Hwa-Yaw Tam[1,2]

[1]Department of Electrical Engineering, The Hong Kong Polytechnic University, Kowloon, Hong Kong, China
[2]Photonics Research Institute, The Hong Kong Polytechnic University, Kowloon, Hong Kong, China
[3]e-mail: dinusha.gunawardena@polyu.edu.hk
[4]e-mail: eechengx@polyu.edu.hk

Received 13 January 2022; revised 21 February 2022; accepted 21 February 2022; posted 22 February 2022 (Doc. ID 453683); published 25 March 2022

We report for the first time, to the best of our knowledge, regenerated polymer optical fiber Bragg gratings (RPOFBGs) in ZEONEX-based polymer optical fibers (POFs). The regeneration temperature can be adjusted using a heat treatment process on the POF before FBG inscription, enabling a scalable improvement of the thermal stability of the RPOFBGs. Thermal sustainability of the RPOFBGs at high temperature conditions was investigated for their prolonged use in diverse environments. Furthermore, these RPOFBGs can withstand strain levels up to 2.8% while maintaining a good linearity, even at temperature of 110°C. The RPOFBGs are capable of short-term operation at elevated temperatures of up to 132°C, which is the standard temperature for steam sterilization with at least a 4 min exposure period. The distinction in the morphologies of the two grades of ZEONEX (E48R and 480R, ZEON Corp.) used to fabricate the optical fiber together with the characteristics of UV irradiated and regenerated gratings is explained using micro-Raman spectroscopy. Collectively, these findings provide new heights for long-term operation of POF Bragg gratings (POFBGs) at elevated temperature environments and would be applicable to a wide range of disciplines.

https://doi.org/10.1364/PRJ.453683

1. INTRODUCTION

In the recent years, fiber Bragg gratings (FBGs) inscribed in polymer optical fibers (POFs) have been increasingly popular among the research community due to their numerous intrinsic features, particularly in biomedical applications [1–3]. In addition to sharing the same virtues of silica-based optical fibers, such as immunity to electromagnetic interference, a light weight, and multiplexing capabilities, POFs are also biocompatible and have low Young's moduli. They are extremely flexible, not brittle in nature, and possess extensively large elongation levels. In the realm of POF-based fiber optic sensing, substantial research has been carried out in the fabrication of POFs based on different grades of polymers; namely, poly (methyl methacrylate) (PMMA) [4], polycarbonate (PC) [5], cyclic transparent optical polymer (CYTOP) [6], and various combinations of them together with other photosensitivity-enhancing dopants including diphenyl disulfide (DPDS) [1] and benzil dimethyl ketal (BDK) [7]. While all the aforementioned polymers have an aptitude for moisture absorption, the advent of a new class of polymers referred to as cyclo olefin polymers (e.g., ZEONEX) and cyclic olefin copolymers (e.g., TOPAS) have demonstrated very low affinity toward water, mitigating the humidity cross sensitivity. This makes them ideal for biomedical applications where measurements are often conducted in aqueous environments.

FBG inscription in these POFs is usually carried out with the use of continuous wave helium cadmium (HeCd) lasers with an operational wavelength of 325 nm, despite their long inscription durations that typically are approximately several minutes for a single FBG [8] compared to a few seconds when using 248 nm excimer lasers [4]. This is aside from circumstances such as the incorporation of the special photosensitive dopant DPDS, which significantly reduces the 325 nm based FBG inscription time to 7 ms [1]. The mechanism responsible for the photosensitivity of undoped PMMA with UV irradiation using the former has proven to be a competitive process between photodegradation and polymerization [9]. On the other hand, UV irradiation by the latter is ascribed to a photolysis process that results in a complete scission of the side chain of PMMA [10]. With the use of low repetition rates and low UV fluences at 248 nm, Bragg gratings below the threshold

of PMMA ablation have been inscribed in PMMA-based microstructured POFs [11]. Furthermore, research findings on high-strain measurements carried out on DPDS-doped PMMA POFs have verified that 325 nm and 248 nm based UV irradiation has a minimal impact on the mechanical properties in the elastic regime [12].

The recent unveiling of FBG inscription in ZEONEX-based, single-mode POFs composed of two grades of ZEONEX (namely, E48R and 480R) in mere nanoseconds using 248 nm UV irradiation can be regarded as a technological breakthrough that lays the foundation for mass production of FBGs in these chemically inert POFs [13]. Their superior drawability, low moisture affinity, and ability to withstand high temperatures make them excellent candidates for high-temperature, humidity-insensitive sensor development. These characteristic features of ZEONEX-based POFs coupled with the innate benefits of POFs could be beneficial in minimally invasive surgeries. For instance, in an extremely stringent minimally invasive procedure such as catheter mediated radiofrequency ablation (RFA), temperatures exceeding 100°C result in the formation of char, and the development of coagulum around the ablation site, which is considered a main surgical drawback [14,15]. This can also lead to undesirable harmful complications such as tissue perforations and steam popping [15]. Hence, real-time temperature monitoring is of utmost importance since it provides critical information on the adequacy of tissue heating, and the prevention of localized blood coagulation and maximization of the lesion size [14].

Although, POFs have distinct benefits compared to glass fibers, their ability to operate at high temperatures is limited by the low glass transition temperature (T_g) of the host material. At temperatures exceeding T_g of the POFs, the main chain of the polymer molecules becomes mobile and leads to a deformation of the polymer material. Regarding survival at elevated temperatures, FBGs inscribed with 325 nm UV irradiation in TOPAS grade 5013 are limited to 110°C [16], in ZEONEX 480R to 123°C [17], and in PC to 125°C [5]. On the other hand, FBGs in PMMA-based POFs fall short at 92°C [18]. High-temperature-resistant gratings referred to as regenerated fiber Bragg gratings (RFBGs) [19] and resurgent regenerated fiber Bragg gratings (R^2FBGs) [20], where grating regeneration and resurgence occur at ∼900°C and ∼1360°C, respectively, have been reported in silica-based fibers. While UV-assisted bond breakage, stress variations, and transient excitation states instigated by the laser are believed to play key roles in grating regeneration or resurgence in silica-based fibers [20,21], the possibility of grating regeneration as well as the impact of stress changes introduced by deep UV irradiation on the high temperature and strain properties of FBGs in POFs remains spheres that are yet to be explored.

In this study, we report, for what we believe is the first time to the best of our knowledge, a new class of Bragg gratings in ZEONEX-based POFs referred to as regenerated polymer optical fiber Bragg gratings (RPOFBGs) that are suitable for high temperature and strain measurements. A thermal treatment process is proposed in an effort to tune the regeneration temperature of these RPOFBGs and a detailed comparison of regeneration characteristics of POFBGs when subjected to different thermal treatments is demonstrated. Furthermore, the thermal stability of these RPOFBGs over a wide range of temperatures is investigated along with the maximum sustainable temperature to assess the operational temperature range of these sensors. Moreover, the strain responses of these RPOFBGs also are extensively characterized at elevated temperatures. Additionally, a structural analysis is conducted with the use of micro-Raman spectroscopy to unravel the underlying mechanisms of grating regeneration in these 248 nm UV irradiated ZEONEX-based POFs. We believe the findings of this study will provide a progressive leap into conceptualization of the dynamics of high-temperature-resistant POFBG technology.

2. THERMAL TREATMENT PROCEDURE

During the fiber drawing process, a rearrangement of the polymer molecules occurs in which they tend to align along the fiber axis [22]. The degree of this alignment is governed by various drawing conditions and the thermal history of the fiber preform, which both contribute toward a residual freezing in stress after the drawing process. Thermal annealing reverts the polymer chains to a thermodynamically favorable configuration that results in stress relaxation and an alteration of the mechanical properties of these POFs. When the local temperature exceeds the shrinking threshold, it can also cause a permanent shrinkage in the fiber [22,23], which will impact the response of the FBG, since the reading of the sensor is directly tied to the Bragg wavelength, and is undesirable for practical implementation. Nevertheless, thermal annealing is not necessarily detrimental. Several studies have used it as a technique to reduce the grating inscription time [4] and tune the Bragg wavelength to a desired wavelength after FBG inscription [5]. Furthermore, improved thermal and strain responses with the absence of hysteresis have been achieved for FBGs inscribed in annealed POFs [23]. Moreover, the shrinking of the fiber can be avoided by annealing the POFs prior to FBG inscription, which also helps to increase the linear operational temperature range of the FBGs [18]. Although, the basic influence of thermal annealing has received partial recognition, it is prudent to conduct a comprehensive study to evaluate the impact of the pre-annealing temperature on the thermal response and stability of FBGs in POFs.

The ZEONEX-based POFs used in this study were fabricated in-house and are composed of two grades of ZEONEX, where the core consists of E48R and cladding of 480R, as illustrated in Fig. 1(a). The core and cladding diameters of the fiber are 9.3 μm and 160 μm, respectively, as shown in Fig. 1(b). The NA of the fiber is 0.16, with a minimum attenuation of 4.5 dB/m at 847.5 nm. The detailed fabrication procedure of these fibers is described in our previous research study [13]. Prior to FBG inscription, four batches of fibers labeled A, B, C, and D were subjected to a thermal treatment process at four different temperatures, 85°C, 105°C, 115°C, and 128°C, respectively, for a time duration of 48 h inside an oven. The FBGs inscribed in the respective POFs were labeled as $POFBG_A$, $POFBG_B$, $POFBG_C$, and $POFBG_D$. It should be noted that when thermally treating the polymer material to attain molecular stress relaxation, T_g of the material

should not be surpassed since temperatures approaching T_g will result in large polymer sections being mobile in contrast to localized molecular movement [24].

3. REGENERATED POLYMER OPTICAL FIBER BRAGG GRATINGS

A. Fabrication of RPOFBGs

POFBGs that were 4 mm long were inscribed in both thermally treated and untreated fibers using a phase-mask technique (Ibsen Photonics) with the aid of a 25 ns pulsed 248 nm KrF excimer laser (BraggStar M, Coherent) simply with the use of two UV pulses with a pulse energy of 50 mJ. The POFBGs were connectorized with silica SMFs for optical coupling using a UV curable adhesive (Norland, NOA 86H). They were then placed inside an in-house fabricated miniature oven consisting of a negative temperature coefficient (NTC) thermistor with a temperature resolution of 0.02°C for a thermal annealing procedure, as illustrated in Fig. 1(c). An external thermocouple was also placed in close proximity to the grating for accurate temperature detection. The reflection spectra of the POFBGs were monitored using an optical sensing interrogator (sm125, Micron Optics) with a wavelength accuracy of 1 pm and a sampling rate of 2 Hz. The spectra were recorded with the aid of a LabVIEW program throughout the annealing process. Figure 1(d) shows the thermal response of an FBG inscribed in a ZEONEX-based POF that was not subjected to any prior thermal treatment process. An initial decay in the peak power is observed with increasing temperature when the temperature is continuously raised from 25°C at a ramping rate of 1°C/min, followed by a sudden increase in the peak power at 70°C. It continues to rise to a level that exceeds its original reflected peak power before plummeting at 100°C. This phenomenon is referred to as regeneration of the POFBG. A further increase in temperature continues to deteriorate the reflected peak power of the newly created RPOFBG. After ~2 h of heating, the

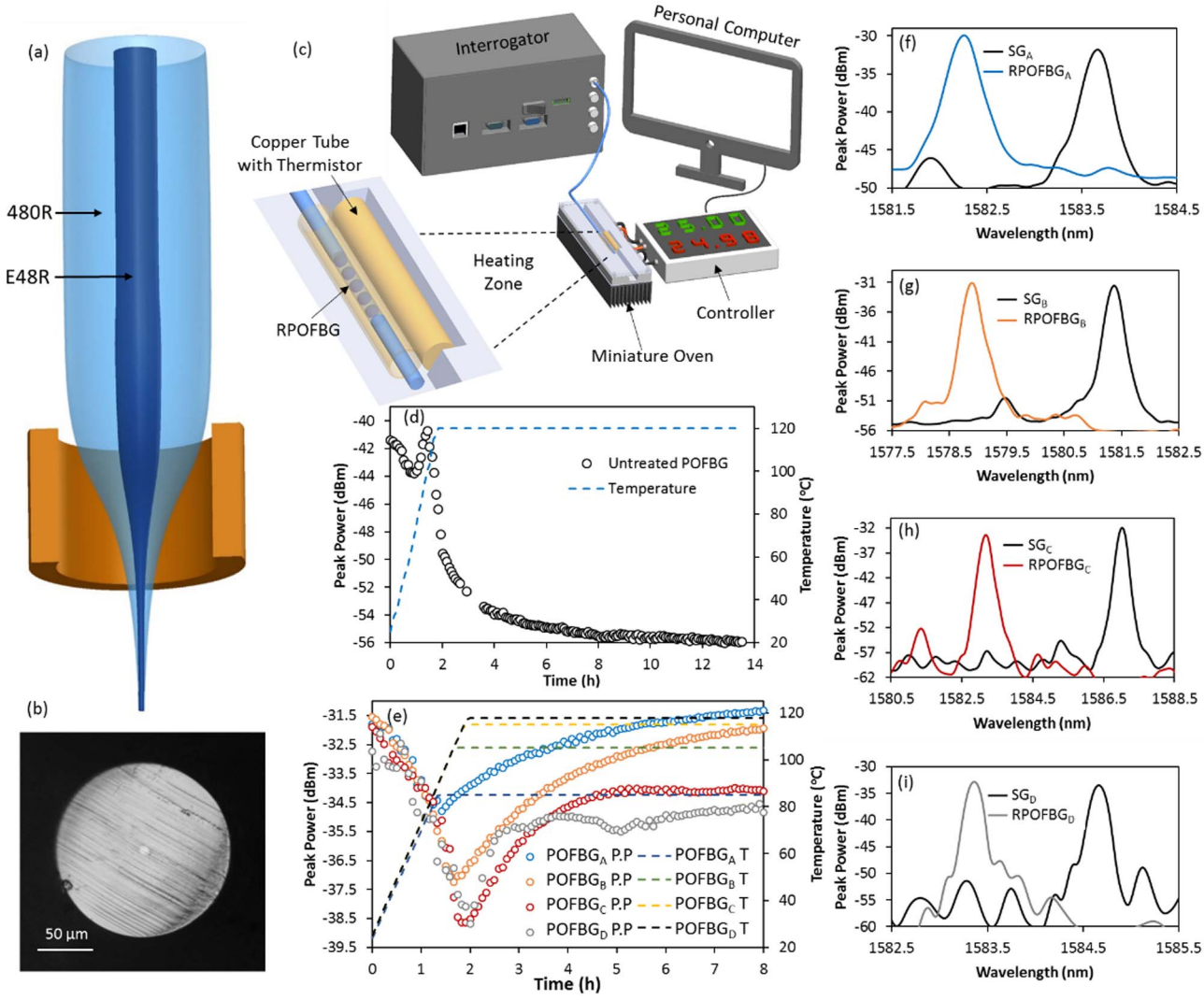

Fig. 1. (a) Schematic illustration of core and cladding compositions and (b) cross-sectional microscopic image of ZEONEX-based POF. (c) Experimental configuration of the thermal annealing setup; evolution of reflected peak power of POFBGs during thermal regeneration inscribed in (d) untreated and (e) thermally treated ZEONEX-based POFs. Reflection spectral profiles of SG_{A-D} and $RPOFBG_{A-D}$ in ZEONEX-based POFs at room temperature that underwent thermal treatment at (f) 85°C, (g) 105°C, (h) 115°C, and (i) 128°C.

temperature was maintained at 120°C for another 11 h and 45 min, which resulted in a further decay of the strength of the RPOFBG.

Afterward, the FBGs inscribed in batches A, B, C, and D also were subjected to the same annealing procedure. Figure 1(e) shows the evolution of the grating reflectivity of $POFBG_X$ (where X denotes A, B, C, and D) inscribed in the four batches of POFs with similar grating strength. It is observed that, with increasing temperature, the reflected peak powers of all the POFBGs gradually degrade due to a decrease in the UV-induced index modulation and the regeneration process is initiated at the temperature at which they were thermally treated, except for that of $POFBG_D$. At the minimum reflected peak powers of these POFBGs, the temperature was dwelled until the reflected peak power of each RPOFBG was stabilized, which was at 85°C, 105°C, 115°C, and 118°C for $POFBG_{A-D}$, respectively. In $POFBG_D$, regeneration occurs at 118°C, which is 10°C below its treated temperature. This suggests that for ZEONEX-based FBGs the ultimate regeneration temperature is 118°C. When sufficient thermal energy is introduced to the polymer material, the molecular chains become mobilized and, at a certain temperature, these molecular chains may tend to relax toward its equilibrium state, becoming amorphous and reorganizing its conformation. This molecular rearrangement also is believed to remove the internal stress. This sequence of events may lead to the regeneration of POFBGs.

Figures 1(f)–1(i) show the spectral comparisons of the original seed gratings (SGs) and the RPOFBGs. With increasing annealing temperatures, the drift in the wavelengths between SG_{A-C} and $RPOFBG_{A-C}$ increases, and wavelength shifts of 1.39 nm, 2.48 nm, and 3.84 nm were recorded for SG_A/$RPOFBG_A$, SG_B/$RPOFBG_B$, and SG_C/$RPOFBG_C$, respectively. However, a wavelength drift of only 1.3 nm is observed for SG_D/$RPOFBG_D$. In addition, as shown in Fig. 1(e), although the reflected peak power tends to decay and restore to a level of ~−35 dBm during grating regeneration of $POFBG_D$, similar to the spectral comparison in Fig. 1(i), a total recovery of it is observed when the RPOFBG is cooled down to ambient temperature. This implies that thermal treatment as high as 128°C, which is only 10°C below the T_g of ZEONEX-based POFs, is sufficient for a stable operation of the RPOFBG. However, thermal treatment exceeding 128°C is not recommended due to the shrinkage of these ZEONEX-based POFs. The permanent blueshift of Bragg wavelengths of these RPOFBGs compared to their respective SGs can be attributed to the relaxation of the polymer chains as a result of the annealing process. When considering the peak power of SGs and RPOFBGs, a higher ratio is observed for $POFBG_A$ compared to the rest, which indicates a higher index modulation ratio $\Delta\eta_{reg}/\Delta\eta_{seed}$ for $POFBG_A$. Table 1 summarizes the thermal history of the fabricated $RPOFBG_{A-D}$.

Table 1. Thermal History of the Fabricated RPOFBGs

Type of RPOFBG	Thermal Treatment Temperature of POFs (°C)	Regeneration Temperature (°C)	Wavelength Shift between SGs and RPOFBGs (nm)
$RPOFBG_A$	85	85	1.39
$RPOFBG_B$	105	105	2.48
$RPOFBG_C$	115	115	3.84
$RPOFBG_D$	128	118	1.30

B. Thermal Sensitivity of RPOFBGs

The temperature sensitivities of the fabricated $RPOFBG_{A-D}$ were investigated by conducting subsequent heating and cooling cycles, as shown in Fig. 2. The temperature was slowly ramped at 1°C/min from the ambient temperature (25°C) to the regeneration temperatures of $RPOFBG_{A-C}$ and cooled back

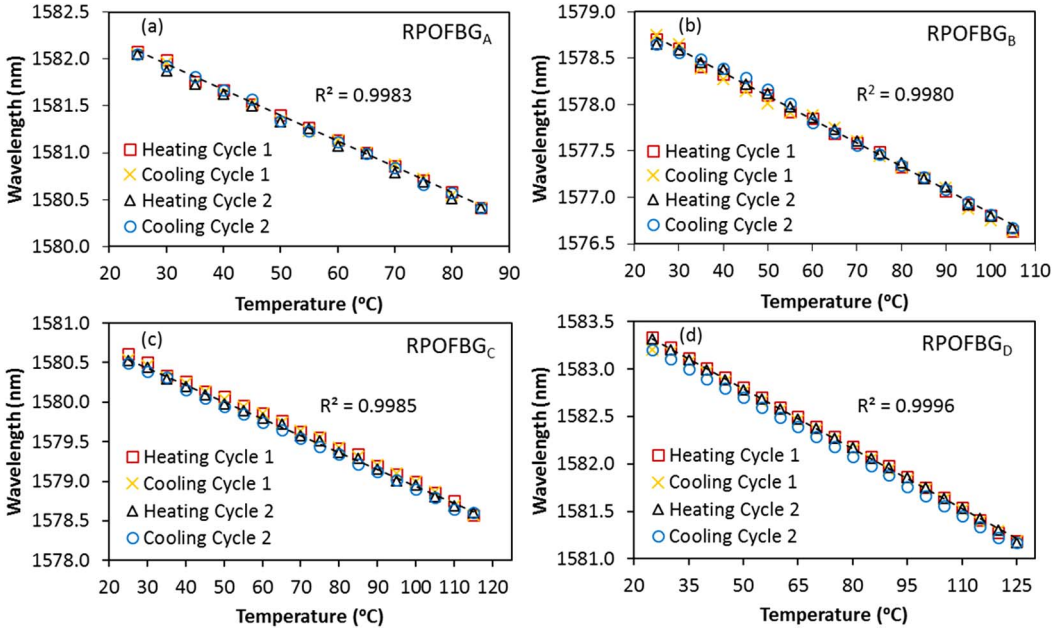

Fig. 2. Temperature measurements for two heating and cooling cycles each: (a) $RPOFBG_A$ from 25°C to 85°C, (b) $RPOFBG_B$ from 25°C to 105°C, (c) $RPOFBG_C$ from 25°C to 115°C, and (d) $RPOFBG_D$ from 25°C to 125°C.

to the ambient temperature. For $RPOFBG_D$, the temperature was raised until 125°C, which is above the 118°C regeneration temperature of the fiber, but is 3°C below its thermal treatment temperature of 128°C. Even at this elevated temperature, $RPOFBG_D$ still exhibits good linearity. Temperature sensitivities of 27, 25.4, 21.8, and 21.3 pm/°C were exhibited by $RPOFBG_A$, $RPOFBG_B$, $RPOFBG_C$, and $RPOFBG_D$, respectively. The decreasing trend in the temperature sensitivities, particularly of $RPOFBG_C$ and $RPOFBG_D$, can be attributed to structural variations occurring in the polymer material due to prolonged exposure at high temperatures, initially during the thermal treatment process of the POFs and subsequently during the thermal regeneration procedure of the POFBGs. Good linearity with the absence of any hysteresis can be observed for $RPOFBG_{A-D}$ with R^2 values of over 99.8% for two temperature cycles of each RPOFBG, which denotes a linear dependence on both the thermal expansion coefficient and thermo-optic coefficient. The dominating negative thermo-optic coefficient of the material results in a blueshift of the Bragg wavelengths with increasing temperatures.

C. Thermal Stability of RPOFBGs

One specific complication associated with the use of POFBGs is their restricted thermal stability, even at temperatures lower than their T_g. Beyond a certain temperature, a rapid decrease in the Bragg wavelength with increasing temperature is observed for POFBGs regardless of the type of polymer material. It should be noted that stability of a Bragg wavelength at any given temperature is also affected by the humidity of the surrounding environment, except for cyclo olefin polymers or copolymers.

Several research studies have attributed this permanent wavelength drift to fiber shrinkage with rising temperatures [16,18,22]. At a controlled humidity level of 10% RH, a rate of Bragg wavelength shift of 0.3 nm/h has been observed for PMMA-based mPOFBGs at a temperature of 80°C after 20 h of annealing [25]. PC-based mPOFBGs have exhibited wavelength shifts of 10.7 nm and 6 nm at annealing temperatures of 120°C (for 24 h) and 130°C (for 12 h), respectively [5]. Humidity-insensitive TOPAS-based mPOFBGs have exhibited a total wavelength drift of 5 nm after 7 h of annealing at 110°C [16]. A total blueshift of 33.7 nm at 120°C for an annealing time of 36 h has been observed for ZEONEX 480R based mPOFBGs [26]. The recent study on ZEONEX-based POF with the combination of E48R/480R has reported a wavelength shift of 11.7 nm after annealing the POFBGs in a two-step process, at 115°C for 20 h and at 125°C for 15 h [17]. Even in POFs that underwent a pre-annealing process at 80°C for two days, a total wavelength drift of ~8 nm was observed in FBGs inscribed in polystyrene-doped, PMMA-based POFs at 85°C after an annealing time duration of 5 h [23]. Table 2 summarizes the thermal stability of these different types of POFs under various annealing conditions.

In spite of the reported efforts of numerous temperature stabilization techniques of POFBGs, analysis on their thermal stability remains orphaned due to the lack of comprehensive research investigations and characterizations on the thermal behavior of these POFBGs at elevated temperatures; hence, there is a missing crucial study for their long-term repetitive usage. Furthermore, the role and impact of a pre-annealing temperature are not yet fully understood. In this context, several experiments were conducted in an attempt to investigate the thermal stability of RPOFBGs at various temperatures. Stepwise heating and cooling procedures were carried out from 25°C to the regeneration temperatures of $RPOFBG_{A-D}$ and back to 25°C in steps of 20°C and with a temperature gradient of 10°C for $RPOFBG_C$ and $RPOFBG_D$ in their final heating step. The temperature was increased and decreased at a ramping rate of 1°C/min and dwelled at each step for 2 h.

Figures 3(a) and 3(b) demonstrate the shift in Bragg wavelengths and normalized reflected peak powers of $RPOFBG_{A-D}$ at different temperatures. The rates of wavelength shift at the regeneration temperatures of $RPOFBG_A$, $RPOFBG_B$, and $RPOFBG_C$ are 0.04, 0.03, and 0.10 nm/h, respectively. When compared to the thermal stability of POFBGs in pre-annealed polystyrene-based PMMA fibers at 85°C [23], the wavelength shift for $RPOFBG_A$ over 2 h was 62 times more stable. However, a wavelength shift of 0.17 nm/h was observed at 115°C for $RPOFBG_D$, annealing at 105°C, which resulted in a wavelength drift of only 0.005 nm/h. Furthermore, from Fig. 3(b), only a slight fluctuation in the reflected peak power is observed for the $RPOFBG_{A-D}$ aside from the ~2 dB non-permanent decay in it at 115°C for both $RPOFBG_C$ and $RPOFBG_D$. Hence, in an attempt to investigate the maximum temperature at which $RPOFBG_{A-D}$ can be thermally stabilized with a minimum drift in the wavelength, an additional characterization was performed, where $RPOFBG_D$ was heated

Table 2. Thermal Stability of POFBGs in Different Types of POFs

Type of POF	Pre-annealing Temperature (°C)	Pre-annealing Time (h)	Annealing Temperature (°C)	Annealing Time (h)	Wavelength Shift (nm)
PMMA mPOF [25]	–	–	80	20	75
PC mPOF [5]	–	–	120	24	10.7
			130	12	6
TOPAS mPOF [16]	–	–	110	7	5
ZEONEX mPOF [26]	–	–	120	36	33.7
ZEONEX E48R/480R [17]	–	–	115	20	11.7
			125	15	
Polystyrene doped PMMA [23]	80	48	85	5	8
ZEONEX E48R/480R (this study)	128	48	110	7	0.18

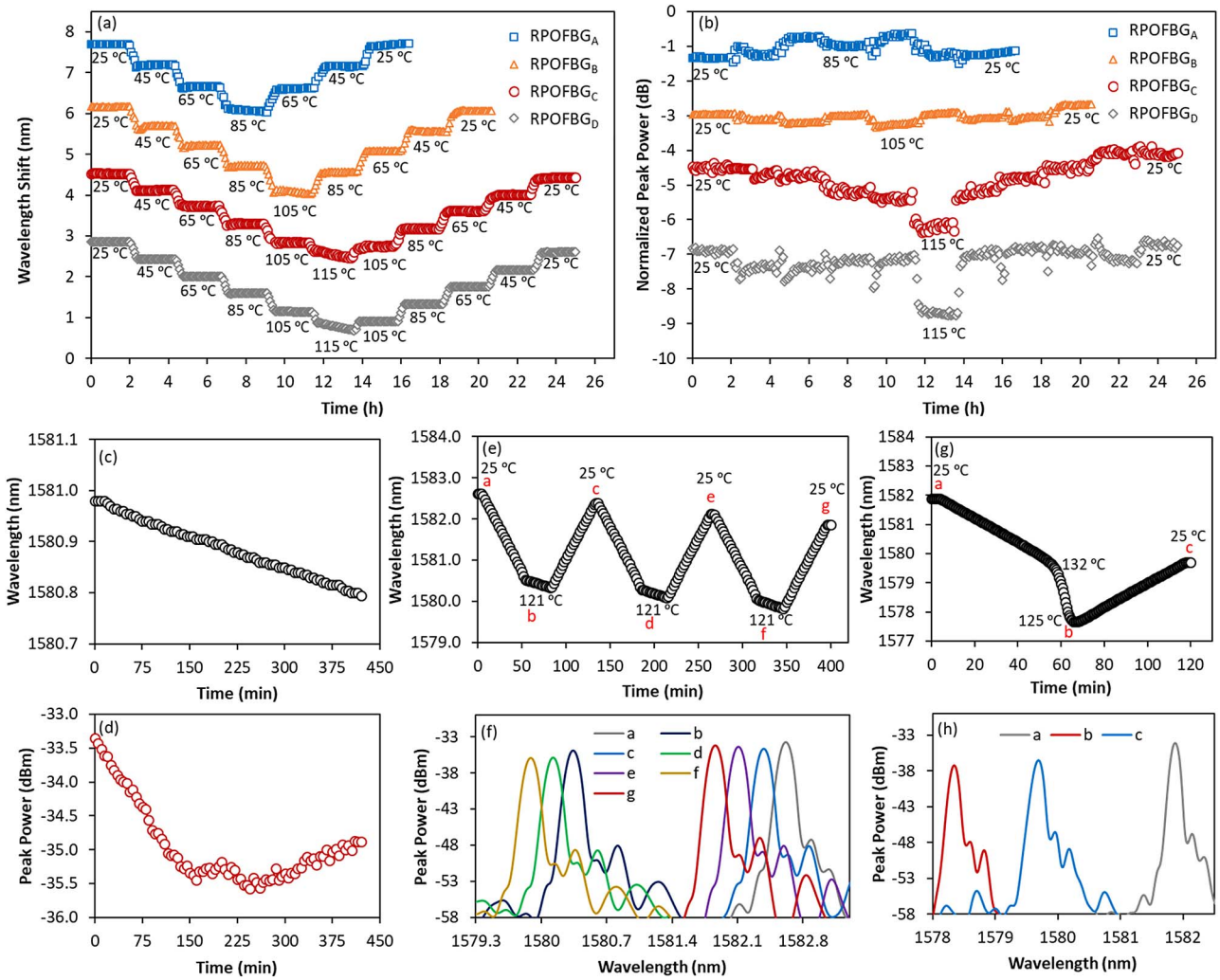

Fig. 3. (a) Normalized Bragg wavelength and (b) peak power stability of RPOFBG$_{A-D}$ during stepwise heating and cooling processes from 25°C to respective regeneration temperatures. Temperature ramping rate is 1°C/min with a dwell time of 2 h at each step. (c) Bragg wavelength shift and (d) corresponding variation in reflected peak power of RPOFBG$_D$ at 110°C over 7 h. (e) Bragg wavelength shifts of RPOFBG$_D$ during three stepwise heating and cooling cycles from 25°C to 121°C and (f) reflection spectrum profiles corresponding to each step, denoted as a–g. (g) Bragg wavelength shift of RPOFBG$_D$ during a single heating and cooling cycle from 25°C to 132°C, and (h) reflection spectrum profiles corresponding to each step, denoted as a–c. Temperature ramping rate is 2°C/min with dwell times of 30 min and 4 min at 121°C and 132°C, respectively.

at 110°C for 7 h. Figures 3(c) and 3(d) show the wavelength shift and the response of the reflected peak power, respectively, at 110°C. A maximum wavelength shift of only 0.18 nm is observed during the 7 h annealing process for RPOFBG$_D$. Compared to the wavelength stability of TOPAS-based mPOFBGs at 110°C [16], it is a ~28-fold improvement, which clearly highlights the significance of the thermal treatment procedure. It also suggests that 110°C is the highest temperature at which ZEONEX-based RPOFBGs can be incorporated for long-term temperature-sensing applications.

Steam sterilization is a commonly used protocol in medical and healthcare facilities where moist heat sterilization is accomplished in autoclaves to destroy microorganisms that include bacteria, fungi, and viruses. A typical standard steam sterilization of surgical instruments and medical devices is achieved using saturated steam at 121°C for 30 min or at 132°C for 4 min [27]. In this regard, to assess the suitability of integrating ZEONEX-based RPOFBGs with medical instruments and implants that undergo steam autoclave procedures, the thermal response and stability of ZEONEX RPOFBGs were investigated at 121°C and 132°C. Figure 3(e) demonstrates the wavelength shifts during three cycles of heating from 25°C to 121°C and back to 25°C at a temperature ramping rate of 1°C/min while maintaining the temperature at 121°C for 30 min. The spectral profiles at each step of the annealing process denoted by a–g are shown in Fig. 3(f). At the positions of b, d, and f, where the temperature is 121°C, an average wavelength drift of 0.2 nm was recorded over 30 min of annealing. As demonstrated in Fig. 3(g), another cycle at 132°C with a dwell time of 4 min also was conducted. A rapid drift in the Bragg wavelength can be observed during the annealing process at 132°C. The wavelength continues to blueshift even during the cooling process until 125°C. Then, there is a resumption of a redshift with decreasing temperatures. Furthermore, an

overall decay of 2.3 dB of the reflected peak power can be observed from the spectral profiles in Fig. 3(h) along with a broadening of the spectra. Compared to spectrum a, an increase of 0.02 nm in the 3 dB spectral bandwidth was recorded for spectrum c. These findings signify that these RPOFBGs in ZEONEX-based POFs can successfully withstand temperatures up to 132°C, which is, to the best of our knowledge, the highest sustainable temperature reported for any type of POFBG. However, successive uses would require the sensor to be recalibrated.

D. Thermal Response of RPOFBGs under Low- and High-temperature Sensing

In light of the aforementioned discoveries, further thermal characterizations were conducted in an attempt to evaluate the characteristic behavior of the RPOFBGs under low- and high-temperature conditions. Therefore, $RPOFBG_D$ was cooled and heated from 24°C to 2°C for two cycles, as shown in Fig. 4(a). A temperature sensitivity of 21.2 pm/°C was obtained for both cycles with a linearity of 99.99%, which confirmed the hysteresis-free operation of the RPOFBG.

Afterward, another sample of $RPOFBG_D$ was continuously heated to investigate its maximum sustainable temperature. From Fig. 4(b), it is clear that beyond 125°C, the linearity of the wavelength response is completely lost and exhibits a drastic drift in the Bragg wavelength. The spectral profiles in Fig. 4(c) demonstrate broadening and severe distortions of the reflection spectra of $RPOFBG_D$ when the heating temperatures approach T_g of ZEONEX E48R (139°C). Hence, it is verified that although the RPOFBGs can successfully withstand temperatures up to 137°C for a short time span, they are best suited to be operated up to 110°C for long-term operations. It should also be noted that even for $RPOFBG_D$, where the POF was initially subjected to a thermal treatment process at 128°C, the linear temperature operation range is limited to only 125°C. Thus far, POFBGs in PC-based POFs have demonstrated the highest operating temperatures of 125°C, but are sensitive to humidity fluctuations [28].

E. Strain Response of RPOFBGs at Various Temperatures

The strain response of the RPOFBGs was calibrated by mechanically elongating them and monitoring the drift of the Bragg wavelength with increasing strain. A supercontinuum source (SC-5, YSL Photonics) and an optical spectrum analyzer (OSA, AQ6370D, Yokogawa) were incorporated to continuously track the reflected peak of each RPOFBG. The fiber

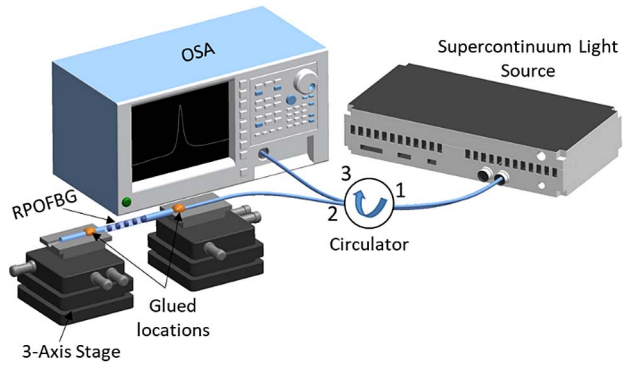

Fig. 5. Configuration of the experimental setup used for strain calibrations.

was glued to two three-axis translation stages (MAX350/M, 1 μm resolution, Thorlabs), each 12 mm apart, as shown in Fig. 5. For $RPOFBG_D$, the fiber was glued to translation stages that were 10 mm apart. High temperature epoxy (353ND, EPO-TEK) was used for the gluing process and was cured at 70°C for 2 h prior to the strain calibrations. Axial strain was manually applied to the RPOFBGs with the use of one of the stages. $RPOFBG_{A-C}$ were subjected to a longitudinal strain of up to 3% in steps of 0.3% elongation, both at the ambient temperature and at temperatures that are 10°C below their regeneration temperatures. $RPOFBG_D$ was subjected to a maximum strain of 2.8%, both at ambient temperature and at 110°C, a milestone unattained, to the best of our knowledge, by previous research. Research progress in this direction was made by Markos *et al.*, where strain sensing was conducted using an FBG inscribed in TOPAS-based fiber at 110°C, up to a strain limit of 0.16% [16]. As illustrated in Figs. 6(a)–6(h), a hysteresis-free linear response is observed for the loading and unloading cycles of each type of RPOFBG, both at room temperature and at high temperatures with an R^2 value of 0.999. Strain sensitivities of 13.45, 13.51, 13.55, and 13.41 nm/% elongation were obtained at room temperature for $RPOFBG_A$, $RPOFBG_B$, $RPOFBG_C$, and $RPOFBG_D$, respectively. At 75°C, 95°C, 105°C, and 110°C, the strain sensitivities were 13.25, 13.41, 13.39, and 13.03 nm/% elongation for $RPOFBG_A$, $RPOFBG_B$, $RPOFBG_C$, and $RPOFBG_D$, respectively. The data shows good repeatability over two cycles of loading and unloading for each RPOFBG at different temperatures.

Figures 6(i)–6(l) show the evolution of the reflection spectra of $RPOFBG_D$ during loading and unloading cycles at the

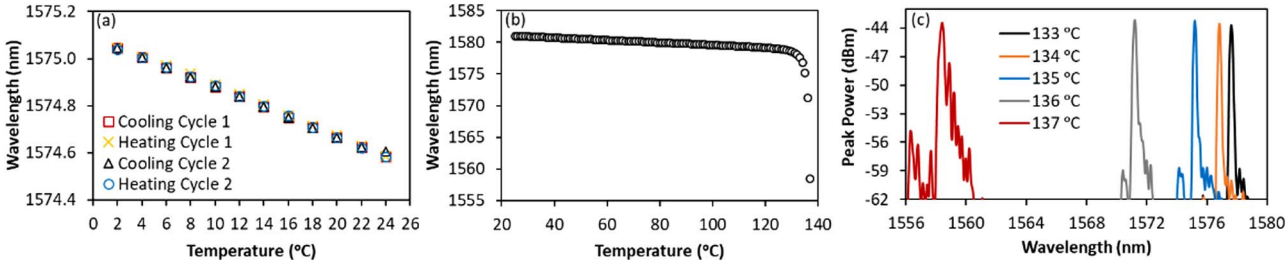

Fig. 4. (a) Temperature sensitivity calibration for two cooling and heating cycles from 24°C to 2°C, (b) wavelength shift with increasing temperature, and (c) corresponding reflection spectrum profiles of $RPOFBG_D$ from 133°C to 137°C. The temperature ramping rate is 1°C/min.

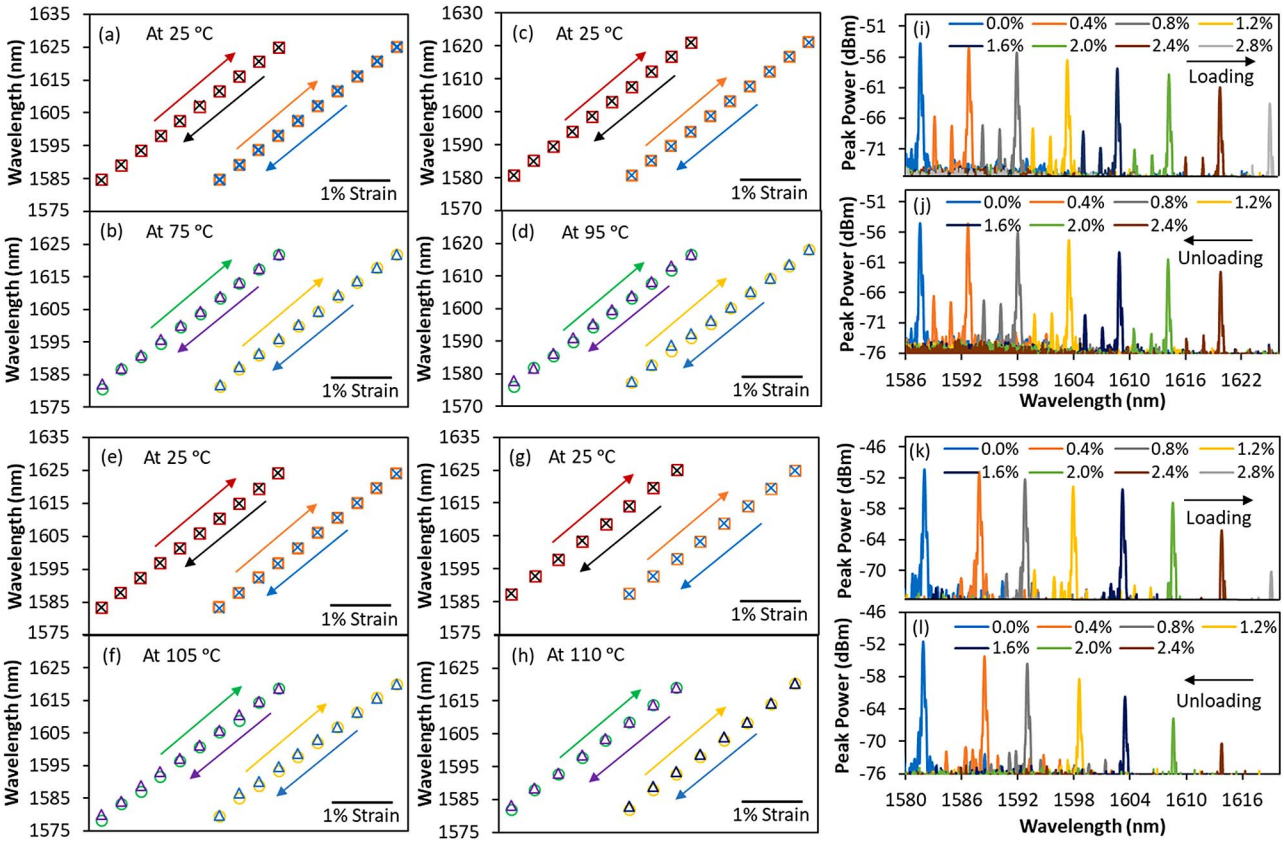

Fig. 6. Strain sensitivity calibrations for two loading and unloading cycles: (a) $RPOFBG_A$ at 25°C and (b) at 75°C; (c) $RPOFBG_B$ at 25°C and (d) at 95°C; (e) $RPOFBG_C$ at 25°C and (f) at 105°C; and (g) $RPOFBG_D$ at 25°C and (h) at 110°C. Reflection spectrum profiles of $RPOFBG_D$ at ambient temperature during (i) loading and (j) unloading cycles and at 110°C during (k) loading and (l) unloading cycles.

ambient temperature and at 110°C, respectively. With increasing elongation, the reflected peak power gradually degrades, with a drastic reduction observed at 2.8% elongation. This decrease in peak power can be attributed to the increased mode propagation loss as a result of the reducing core size when subjected to high longitudinal strain. However, during the unloading cycles the reflected peak power appears to recover, suggesting that no permanent damage is introduced to the RPOFBGs within the strain range.

F. Structural Analysis through Micro-Raman Spectroscopy

To elucidate the morphology of core and cladding materials in ZEONEX-based POFs used in this study and to evaluate the dynamics of grating regeneration, three different batches of ZEONEX-based POF samples subjected to different test conditions were prepared. The first batch consisted of unannealed segments of ZEONEX POFs. The second batch underwent a thermal treatment procedure at 115°C for 48 h and was subsequently subjected to UV irradiation, identical to the process that was used to fabricate $POFBG_C$. Afterward, the second batch was annealed at 115°C for 6 h to produce the third batch, following the regeneration process used to create $RPOFBG_C$. Subsequently, fiber cross sections from each of these batches were examined with the use of a confocal Raman imaging microscope (alpha300 R, WITec) equipped with an excitation laser at 532 nm that delivered 2 mW with a finely focused laser spot size of ~2 μm to the surface of the sample where light guidance occurred through a dry 50× objective (0.75 NA, EC Epiplan, Zeiss). It should be noted that this laser power intensity did not introduce any damage to the POF samples being investigated. Spectra with good SNR were obtained in the 200–4100 cm^{-1} wavenumber range with 10 accumulations of 0.5 s integration time. A computer-controlled, high-precision *XYZ* translation stage was used for confocal mapping, and all the spectra gathered were analyzed using WITec's Project FIVE software.

Figures 7(a)–7(d) show the Raman spectra of the unannealed core (E48R) and cladding (480R) of ZEONEX POFs, where their vibrational modes are assigned to various vibrational regions. The inset shows the generic chemical structure of ZEONEX cyclo olefin polymers, where two substituents R_1 and R_2 are attached to a cyclopentane synthesized through norbornene ring-opening metathesis polymerization (ROMP) and hydrogenation [29]. Raman peak identifications were carried out based on the Raman spectra of different types of polymers available in literature [30–32]. C-C bending (δ) and stretching (ν) vibrational modes are assigned to low wavenumbers from 300 to 1150 cm^{-1}, with rocking (ρ), twisting (τ), and bending C-H bands to wavenumbers from 1150 to 1500 cm^{-1} [31]. Symmetrical (ν_s) and asymmetrical (ν_{as}) stretchings of C-H bands are attributed to higher wavenumbers 2800–3000 cm^{-1}.

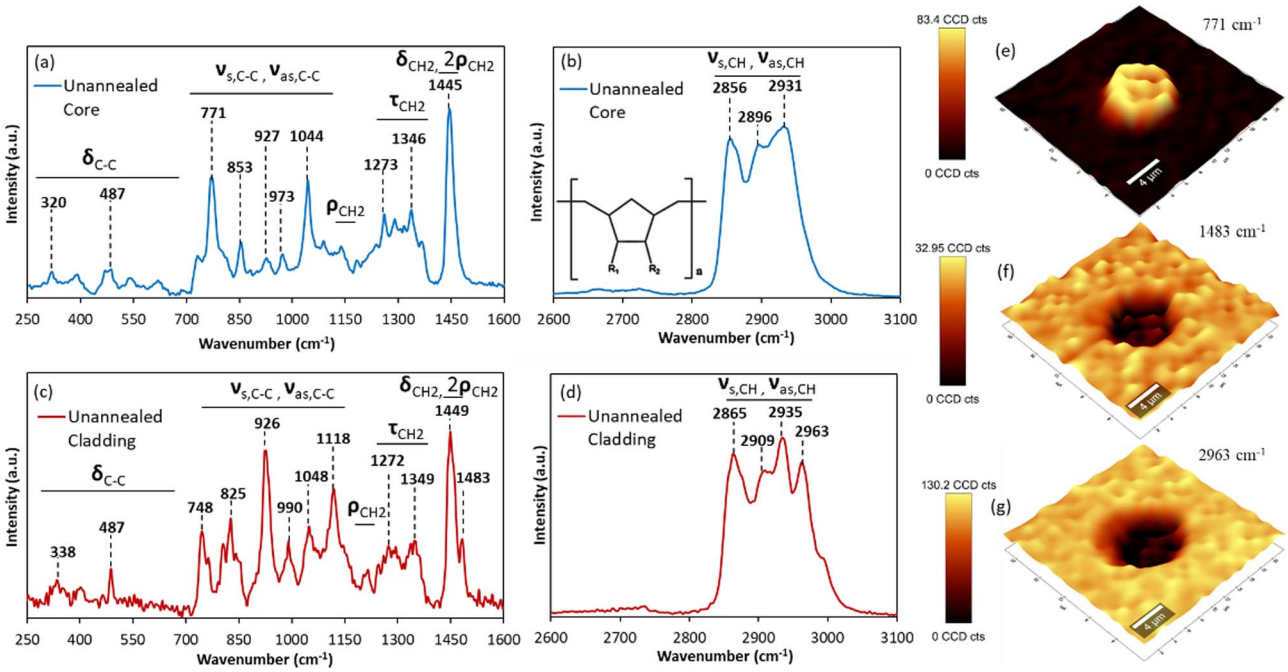

Fig. 7. Raman spectra of ZEONEX material in the core (E48R) from (a) 250 to 1600 cm^{-1} and (b) 2600 to 3100 cm^{-1} and cladding (480R) from (c) 250 to 1600 cm^{-1} and (d) 2600 to 3100 cm^{-1}. Anticipated vibrational mode ranges are denoted. Confocal maps of an unannealed fiber cross section corresponding to Raman peaks at (e) 771 cm^{-1}, (f) 1483 cm^{-1}, and (g) 2963 cm^{-1}. Inset in (b) indicates the chemical structure of ZEONEX cyclo olefin polymer.

The variations in the two grades of ZEONEX are clearly visible from Figs. 7(a)–7(d). The peak present at 771 cm^{-1} in the core of ZEONEX POF responsible for C-C stretching is not visible in the cladding. Furthermore, the shoulder developed at 1483 cm^{-1} attributed to bending of CH_2 and the peak at 2963 cm^{-1} assigned to the stretching of C-H in the cladding are absent in the core. These observations are apparent from the confocal maps of the fiber cross section shown in Figs. 7(e)–7(g), where a notably high intensity is observed in the core, denoting the lack of 771 cm^{-1} vibration in the cladding and the low intensity dips in the core and demonstrating the absence of 1483 and 2963 cm^{-1} vibrations. These differences in the core and cladding can be attributed to variations arising from R_1 and R_2 substituents in E48R and 480R.

Afterward, the variations between the UV irradiated and regenerated samples were investigated in both the core and cladding of the fiber, as shown in Figs. 8(a)–8(d). The peak shift in the Raman spectra is associated with stress changes [33] in the polymer material and, therefore, a series of Raman spectra were acquired from across the fiber cross section. An overall shift in the Raman peaks and a decrease in the widths of the vibrational bands can be observed both in the core and the cladding of the regenerated sample compared to that of the sample subjected to UV irradiation. The insets further emphasize these changes. A slight decay in the peak intensities is observed in the regenerated core and cladding as well. Moreover, a prominent growth of the Raman peak at 1141.5 cm^{-1} [Fig. 8(c)] responsible for C-C stretching vibrations is also observed in the cladding of the regenerated sample. The presence of these Raman shifts in both the core and cladding of the regenerated samples suggests the ability of the amorphous phases to realign and alter their polymer chains irreversibly, depending on the thermal variations, which results in an overall stress change in the fiber. According to Fig. 8(e), spectra stemming from continuous points of the core and cladding regions of the regenerated POF sample show an appreciable shift in the Raman peak, 2849 cm^{-1} common to both grades of ZEONEX, and is responsible for C-H stretching, demonstrating the stress that exists in the core cladding interface of the fiber.

4. CONCLUSIONS

In this study, we have presented the discovery of FBG regeneration in ZEONEX-based POFs, which arises at various temperature regimes and is heavily reliant on thermal treatment procedures conducted prior to FBG inscription. Comprehensive thermal investigations were carried out to evaluate the sensitivity and wavelength stability of these RPOFBGs at different temperatures together with their spectral evolutions. These RPOFBGs are suitable for long-term temperature operations up to 110°C, where an impressive wavelength drift of only 0.18 nm/h was recorded at 110°C. This is a 28-fold advancement compared to that of TOPAS-based POFBGs. The results accentuate the importance of the thermal treatment procedure of the POFs preceding FBG inscription. A survival temperature of 137°C was recorded for the RPOFBG that underwent a thermal treatment process at 128°C at which substantial wavelength drifts occur that indicate its suitability simply for short-term usage (up to 4 min) at 132°C. This is the highest feasible temperature reported for a POFBG, regardless of the type of polymer material.

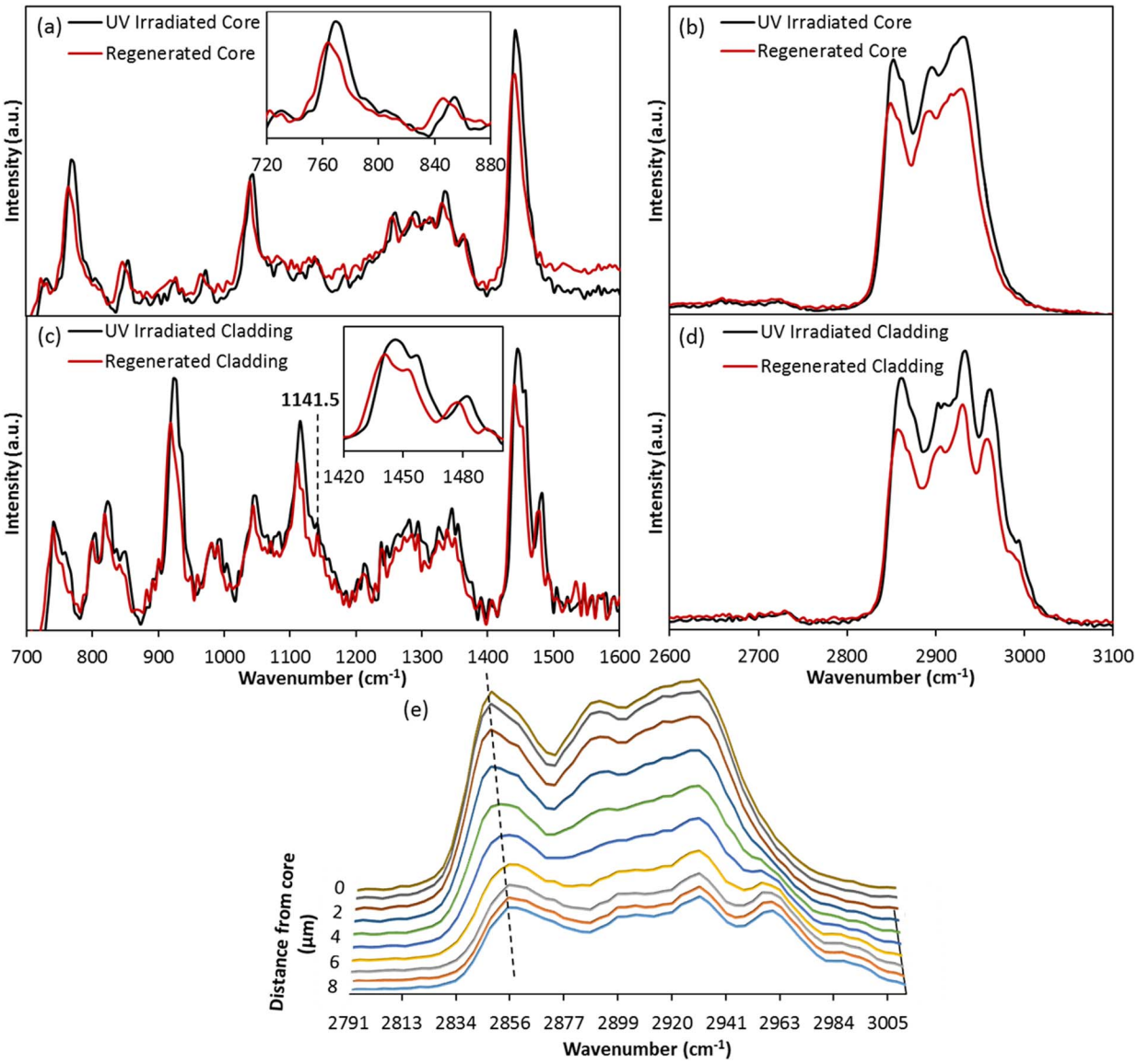

Fig. 8. Comparison of Raman spectra between UV irradiated and regenerated fiber cross sections in the core from (a) 700 to 1600 cm^{-1} (inset shows an enlarged view of the peaks corresponding to C-C stretching vibrations) and (b) 2600 to 3100 cm^{-1}, and in the cladding from (c) 700 to 1600 cm^{-1} (inset shows an enlarged view of the peaks corresponding to CH_2 bending and rocking vibrations) and (d) 2600 to 3100 cm^{-1}. (e) Raman spectra of continuous points from center of the regenerated fiber core to the inner cladding up to 9 μm in steps of 1 μm. Center of the core is referred to as the 0 μm position. The dashed line denotes the shift of the Raman peak.

Additionally, the axial strain properties of the RPOFBGs were also inspected at high temperatures, up to a strain limit of 3%. The experimental findings indicate that strain measurements of up to 2% are recommended at 110°C, because exceeding this strain limit leads to considerable degradations in the spectrum profile of the RPOFBG. Furthermore, a structural analysis on the two grades of ZEONEX (E48R and 480R) in the core and cladding of the POFs was carried out with comparative elucidations of the spectral variations of UV irradiated and regenerated samples with the aid of micro-Raman spectroscopy. The overall shift in the Raman peaks of the regenerated fiber core and cladding compared to that of UV irradiated samples suggests that regeneration of POFBGs is largely driven by the relaxation of dominant stresses through thermal annealing. Thus, we address the speculations and controversy of potential long-term use of POFBGs at elevated temperatures here and have attempted to close the research gap on the investigation of a maximum sustainable temperature of ZEONEX-based POFBGs. We believe that the merits of this study will undoubtedly shape the future of biomedical sensing applications that require low stiffness levels, biocompatibility, and the ability to withstand high temperature and strain levels.

Funding. RGC General Research Fund (15210019); Department of Science and Technology of Guangdong Province (P0034432).

Disclosures. The authors declare no conflicts of interest.

Data Availability. Data underlying the results presented in this paper are not publicly available at this time but may be obtained from the authors upon reasonable request.

REFERENCES

1. J. Bonefacino, H.-Y. Tam, T. S. Glen, X. Cheng, C.-F. J. Pun, J. Wang, P.-H. Lee, M.-L. V. Tse, and S. T. Boles, "Ultra-fast polymer optical fibre Bragg grating inscription for medical devices," Light Sci. Appl. **7**, 17161 (2018).
2. S. Koyama, Y. Haseda, H. Ishizawa, F. Okazaki, J. Bonefacino, and H.-Y. Tam, "Measurement of pulsation strain at the fingertip using a plastic FBG sensor," IEEE Sens. J. **21**, 21537–21545 (2021).
3. C. Broadway, R. Min, A. G. Leal-Junior, C. Marques, and C. Caucheteur, "Toward commercial polymer fiber Bragg grating sensors: review and applications," J. Lightwave Technol. **37**, 2605–2615 (2019).
4. C. A. F. Marques, A. Pospori, G. Demirci, O. Çetinkaya, B. Gawdzik, P. Antunes, O. Bang, P. Mergo, P. André, and D. J. Webb, "Fast Bragg grating inscription in PMMA polymer optical fibres: Impact of thermal pre-treatment of preforms," Sensors **17**, 891 (2017).
5. A. Fasano, G. Woyessa, P. Stajanca, C. Markos, A. Stefani, K. Nielsen, H. K. Rasmussen, K. Krebber, and O. Bang, "Fabrication and characterization of polycarbonate microstructured polymer optical fibers for high-temperature-resistant fiber Bragg grating strain sensors," Opt. Mater. Express **6**, 649–659 (2016).
6. A. Theodosiou and K. Kalli, "Recent trends and advances of fibre Bragg grating sensors in CYTOP polymer optical fibres," Opt. Fiber Technol. **54**, 102079 (2020).
7. X. Cheng, J. Bonefacino, B. O. Guan, and H. Y. Tam, "All-polymer fiber-optic pH sensor," Opt. Express **26**, 14610–14616 (2018).
8. I.-L. Bundalo, K. Nielsen, C. Markos, and O. Bang, "Bragg grating writing in PMMA microstructured polymer optical fibers in less than 7 minutes," Opt. Express **22**, 5270–5276 (2014).
9. D. Sáez-Rodríguez, K. Nielsen, O. Bang, and D. J. Webb, "Photosensitivity mechanism of undoped poly(methyl methacrylate) under UV radiation at 325 nm and its spatial resolution limit," Opt. Lett. **39**, 3421–3424 (2014).
10. C. Wochnowski, S. Metev, and G. Sepold, "UV-laser-assisted modification of the optical properties of polymethylmethacrylate," Appl. Surf. Sci. **154**, 706–711 (2000).
11. R. Oliveira, L. Bilro, and R. Nogueira, "Bragg gratings in a few mode microstructured polymer optical fiber in less than 30 seconds," Opt. Express **23**, 10181–10187 (2015).
12. J. Bonefacino, X. Cheng, C.-F. J. Pun, S. T. Boles, and H.-Y. Tam, "Impact of high UV fluences on the mechanical and sensing properties of polymer optical fibers for high strain measurements," Opt. Express **28**, 1158–1167 (2020).
13. X. Cheng, D. Gunawardena, C. F. Pun, J. Bonefacino, and H. Y. Tam, "Single nanosecond-pulse production of polymeric fiber Bragg gratings for biomedical applications," Opt. Express **28**, 33573–33583 (2020).
14. J. L. Dinerman, R. D. Berger, and H. Calkins, "Temperature monitoring during radiofrequency ablation," J. Cardiovasc. Electrophysiol. **7**, 163–173 (1996).
15. M. Zaltieri, C. Massaroni, F. M. Cauti, and E. Schena, "Techniques for temperature monitoring of myocardial tissue undergoing radiofrequency ablation treatments: an overview," Sensors **21**, 1453 (2021).
16. C. Markos, A. Stefani, K. Nielsen, H. K. Rasmussen, W. Yuan, and O. Bang, "High-T_g TOPAS microstructured polymer optical fiber for fiber Bragg grating strain sensing at 110 degrees," Opt. Express **21**, 4758–4765 (2013).
17. G. Woyessa, H. K. Rasmussen, and O. Bang, "Zeonex–a route towards low loss humidity insensitive single-mode step-index polymer optical fibre," Opt. Fiber Technol. **57**, 102231 (2020).
18. K. E. Carroll, C. Zhang, D. J. Webb, K. Kalli, A. Argyros, and M. C. Large, "Thermal response of Bragg gratings in PMMA microstructured optical fibers," Opt. Express **15**, 8844–8850 (2007).
19. S. Bandyopadhyay, J. Canning, M. Stevenson, and K. Cook, "Ultrahigh-temperature regenerated gratings in boron-codoped germanosilicate optical fiber using 193 nm," Opt. Lett. **33**, 1917–1919 (2008).
20. D. S. Gunawardena, O. kit Law, Z. Liu, X. Zhong, Y.-T. Ho, and H.-Y. Tam, "Resurgent regenerated fiber Bragg gratings and thermal annealing techniques for ultra-high temperature sensing beyond 1400°C," Opt. Express **28**, 10595–10608 (2020).
21. J. Canning, "Regeneration, regenerated gratings and composite glass properties: the implications for high temperature micro and nano milling and optical sensing," Measurement **79**, 236–249 (2016).
22. P. Stajanca, O. Cetinkaya, M. Schukar, P. Mergo, D. J. Webb, and K. Krebber, "Molecular alignment relaxation in polymer optical fibers for sensing applications," Opt. Fiber Technol. **28**, 11–17 (2016).
23. W. Yuan, A. Stefani, M. Bache, T. Jacobsen, B. Rose, N. Herholdt-Rasmussen, F. K. Nielsen, S. Andresen, O. B. Sørensen, K. S. Hansen, and O. Bang, "Improved thermal and strain performance of annealed polymer optical fiber Bragg gratings," Opt. Commun. **284**, 176–182 (2011).
24. A. Pospori, C. A. F. Marques, D. Sáez-Rodríguez, K. Nielsen, O. Bang, and D. J. Webb, "Thermal and chemical treatment of polymer optical fiber Bragg grating sensors for enhanced mechanical sensitivity," Opt. Fiber Technol. **36**, 68–74 (2017).
25. G. Woyessa, K. Nielsen, A. Stefani, C. Markos, and O. Bang, "Temperature insensitive hysteresis free highly sensitive polymer optical fiber Bragg grating humidity sensor," Opt. Express **24**, 1206–1213 (2016).
26. G. Woyessa, A. Fasano, C. Markos, A. Stefani, H. K. Rasmussen, and O. Bang, "Zeonex microstructured polymer optical fiber: fabrication friendly fibers for high temperature and humidity insensitive Bragg grating sensing," Opt. Mater. Express **7**, 286–295 (2017).
27. S. Lerouge, "Sterilisation and cleaning of metallic biomaterials," in *Metals for Biomedical Devices* (Woodhead Publishing, 2010), pp. 303–326.
28. G. Woyessa, A. Fasano, C. Markos, H. K. Rasmussen, and O. Bang, "Low loss polycarbonate polymer optical fiber for high temperature FBG humidity sensing," IEEE Photon. Technol. Lett. **29**, 575–578 (2017).
29. M. Yamazaki, "Industrialization and application development of cycloolefin polymer," J. Mol. Catal. A Chem. **213**, 81–87 (2004).
30. J. Forsyth, J. M. Pereña, R. Benavente, E. Pérez, I. Tritto, L. Boggioni, and H. H. Brintzinger, "Influence of the polymer microstructure on the thermal properties of cycloolefin copolymers with high norbornene contents," Macromol. Chem. Phys. **202**, 614–620 (2001).
31. A. A. Leal, J. P. Best, D. Rentsch, J. Michler, and R. Hufenus, "Spectroscopic elucidation of structure-property relations in filaments melt-spun from amorphous polymers," Eur. Polym. J. **89**, 78–87 (2017).
32. M. Glotin and L. Mandelkern, "A Raman spectroscopic study of the morphological structure of the polyethylenes," Colloid Polym. Sci. **260**, 182–192 (1982).
33. R. J. Young, "Monitoring deformation processes in high-performance fibres using Raman spectroscopy," J. Text. Inst. **86**, 360–381 (1995).